SIMP–LEX: Systematic Geometry Variation Using Thrust Balance Measurements

IEPC-2007-168

Presented at the 30th International Electric Propulsion Conference, Florence, Italy
September 17-20, 2007

Anuscheh Nawaz[*], Georg Herdrich[†], Helmut Kurtz[‡] and Tony Schönherr[§]
Institut für Raumfahrtsysteme, Universität Stuttgart, 70569, Germany

and

Monika Auweter-Kurtz[¶]
Universität Hamburg, Edmund -Siemers -Allee 1, Hamburg, Germany

The instationary magnetoplasmadynamic thruster SIMP-LEX is being optimized and characterized at the Institute of Space Systems, IRS in Stuttgart. This thruster is a parallel plate, side fed pulsed plasma thruster, developed to serve as main propulsion system for the lunar mission BW1. Within this paper, setup, methods and results of the thrust balance developed for SIMP-LEX characterization, will be shown. The setup and calibration of the thrust balance is described in detail along with the ideal case analytical description of the pendulum movement. The calibration of the thrust balance could not yet be completed, so only qualitative trends and minimal values of the impulse bit and exhaust velocity can be shown here. The impulse bit and mass bit results presented are part of a systematic approach aimed at characterizing the iMPD thruster. The test matrix for this campaign includes changes in capacitor voltage, electrode width, distance between the electrodes, flared or parallel and rectangular or tongue shaped electrodes. The different configurations were compared by measuring their impulse bit and mass bit. Both the impulse bit and mass bit are highest for the highest capacitor voltage and greatest distance between the electrodes. The exhaust velocity calculated from this data however shows the opposite trend: The smallest capacitor voltage and distance between the electrodes results in the highest mean exhaust velocity. Concerning the width of the electrodes, an optimum regarding the impulse bit was found at 40 mm, using the 21 mm distance between electrodes. Both flared and tongue shaped electrodes increase the impulse bit as well as the exhaust velocity.

[*]Doctoral Candidate at the Institute of Space Systems, Electric Propulsion, nawaz@irs.uni-stuttgart.de.
[†]Section Lead Space Transportation, Institute of Space Systems, herdrich@irs.uni-stuttgart.de.
[‡]Head of Laboratory, Institute of Space Systems, kurtz@irs.uni-stuttgart.de.
[§]Research student, schoenherr@irs.uni-stuttgart.de
[¶]President Universität Hamburg.

Nomenclature

A	Amplitude of Oscillation
B	Magnetic Field
d	Electrode Width
D	Torsion Spring Constant
E_0	Bank Energy Stored in Capacitors
E_I	Energy from Impulse
g	Gravitational Constant
h	Distance between Electrodes
h_m	Maximum Height Gained at Center of Mass during Oscillation
I_{bit}	Impuls Bit Delivered by Thruster
J	Current during Discharge
L_0	Inductivity of Thruster, Short Circuited
ΔL	Change in Inductivity through Movement of Plasma Sheet
l_A	Distance from Axis to Point of Deflection Measurement
l_F	Distance from Axis to Point of Force
l_m	Distance from axis to Equivalent Center of Mass
m	Mass of Pendulum
m_{bit}	Mass bit Ablated during One Pulse
T	Time of Acceleration of Pendulum
U_0	Initial Voltage of Capacitors
α	Flare Angle of Electrodes
φ_0	Maximum Angle of Deflection
η_e	Electric Efficiency of Thruster
τ	Duration of Pulse
Θ	Moment of Inertia

I. Introduction

The instationary MPD (iMPD, also referred to as PPT) thruster SIMP-LEX is being designed as part of the institute's endeavor to place the 200 kg satellite BW1 in a lunar orbit. This all electric mission will include two electric propulsion systems, the arcjet system TALOS[1] for phases during the mission requiring higher thrust, and a cluster of instationary MPD thrusters as main propulsion system.[2]

The working principle of an iMPD thruster is shown in Fig. 1 and described in detail in literature,[3].[4]

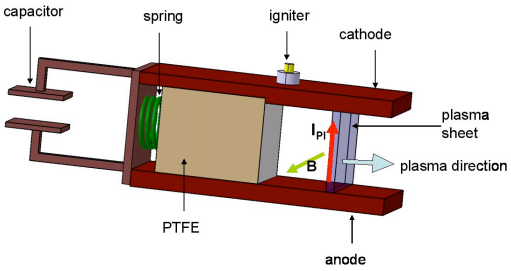

Figure 1. Working principle of a iMPD parallel plate thruster using solid propellant.

BW1 poses certain demands on its main propulsion system. Apart from being a low weight, robust, easy to integrate system, the iMPD cluster will also have to provide BW1 with a Δv of about 5000 m/s, and hence will need a lifetime expectation unprecedented for iMPDs so far. In addition, propellant storage for this mission poses a challenge. For SIMP-LEX, it was decided to feed the propellant through a helix shape which includes feeding propellant from the side. SIMP-LEX is a parallel plate thruster using solid propellant PTFE[5] (Polytetrafluorethylene, *Teflon®*), see Figs. 2 and 3. Its capacitor bank stores up to 80 J in 2000 V, 40 μF foil capacitors. All conducting parts consist of copper. The semiconductor spark plug receives 1000 V and triggers the capacitor discharge. The setup of the thruster configuration allows for easy change of electrode width and distance between the electrodes.

The variations made during the parametric investigation are summarized in Tab. 1. The bank energy E_0 was changed with the capacitor voltage U_0. The electrodes' width d was changed as well as the distance between the electrode plates h. The length of the electrodes was varied in order to investigate the influence on the exhaust velocity. In addition, an increase in change in inductivity ΔL was enforced by flaring the electrodes by an angle of α as well as using a tongue shape.

Propellant feed	side-fed
Voltage, V	1500, 1800, 2000
Capacitance, μF	40
Electrode width, mm	20, 40, 60
Distance between electrodes, mm	21, 36, 42
Length of electrodes, %	75, 100
Flare, $^\circ$	0, 10, 20, 30
Tongue shape	yes, no

Table 1. Table of test configurations compared

The effect of increasing ΔL can be estimated through the very simple slug model.[3] The electrical efficiency η_e is defined as

$$\eta_e = \frac{1}{2}\frac{\int_\tau^0 J^2\,\dot{L}\,dt}{E_0}. \tag{1}$$

Here τ is the total time of one pulse and $\dot{L}$ is the change of inductivity L over time. The current J flows when the capacitor bank of initial energy E_0 discharges. The upper boundary for this efficiency is estimated through the following inequality

$$\eta_e < \frac{\Delta L}{L_0}, \tag{2}$$

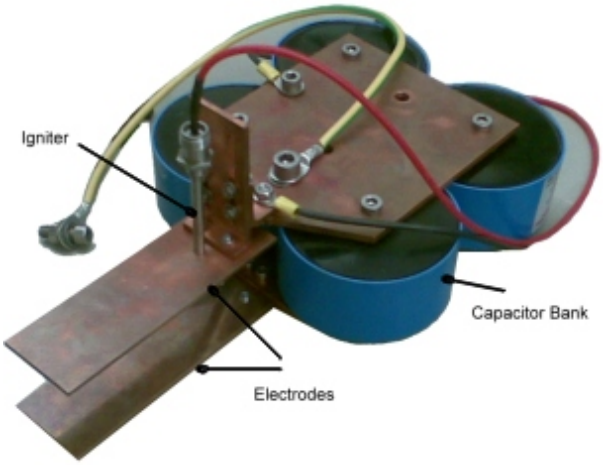

Figure 2. Setup of SIMP-LEX.

Figure 3. SIMP-LEX during one pulse for flared, tongue shaped electrode configuration.

where L_0 is the inductivity of the thruster when short-circuited at the initial position of the plasma. Since L_0 is a fixed value for each thruster, the electric efficiency can be mainly influenced by increasing ΔL. This was done by introducing tongue (or triangular) shaped electrodes and an electrode flare to the thruster setup, as seen in Fig. 3. These geometric changes were investigated theoretically through

$$\Delta L = \frac{\int B\, dA}{J}. \tag{3}$$

Here B is the magnetic field between the electrodes and A is the surface the circuit encircles. Since this surface changes with the position x of the plasma along the electrodes, the inductivity is a function of this position as shown in figures 4 and 5. In Fig. 4 the change in inductivity is plotted across the plasma position for different flare angles. In Fig. 5 the parameter varied is the angle at which the electrode is sharpened. 100% d_0 refers to rectangular electrodes, 0% d_0 electrodes mean the sides of the electrodes form an isosceles triangle, 87 mm behind the exit plane of the *Teflon*® bars. From these figures it becomes clear that tongue shaped electrodes as well as flared electrodes lead to a considerable rise in change of inductivity and hence in electric efficiency. This fact is independent of the initial inductivity of the thruster L_0. Consequently, both setup modifications were tested and compared regarding their change in impulse and exhaust velocity compared to the parallel, rectangular configuration.

As a result of its application on BW1, it is fundamental to precisely know the impulse bit delivered by SIMP-LEX as well as to optimize SIMP-LEX toward higher exhaust velocities. In a first important step, the thruster's geometric and electric parameters were investigated by placing the SIMP-LEX on a thrust pendulum. In order to obtain information on the mean exhaust velocity, the mass bit was measured for each of these configurations.

II. Methods and Setup of Impulse Measurement

The impulse bit of SIMP-LEX was measured for the various parameter settings of the test matrix through a vertical pendulum. The deflection caused by a single shot was recorded with an optical measurement device at the bottom of the pendulum arm. This was done by correlating the impulse bit delivered from the thruster with the amplitude of the deflection. In order to capture impulse bits in the region of μNs, it is important to design the pendulum as frictionless as possible. Fig. 6 shows the thrust balance. It is suspended from two torsion springs. These springs also serve as feed through for charging the capacitor bank. The power supply of the igniter is placed on the pendulum and can be triggered through a window of the vacuum chamber via infrared remote. This design makes it possible for the pendulum to be free from any cables or wires constricting its movement or dissipating energy. This becomes evident after deflection: It takes about $6h$ for the movement to die down if the installed eddy current brakes are not engaged. The thruster is mounted on

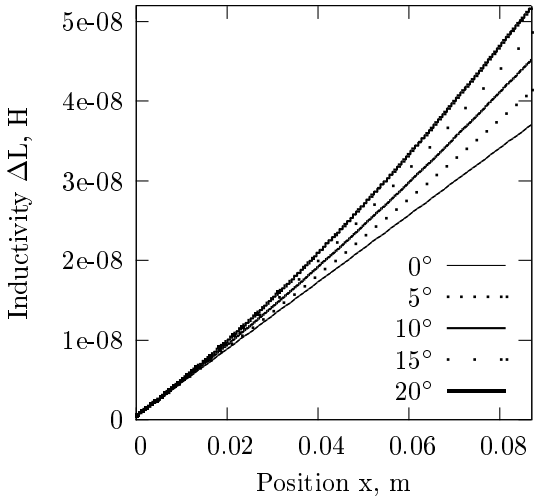

Figure 4. Inductivity over position for different flare angles

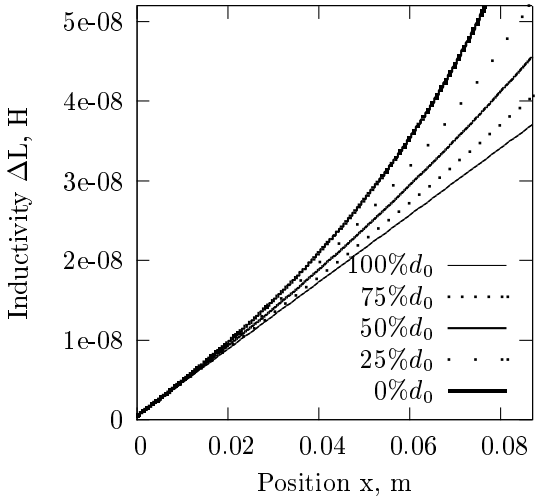

Figure 5. Inductivity over position for different aspect ratios

the pendulum structure - its position can be centered underneath the pendulum axis. The optical deflection unit measures by sending infrared waves onto a measurement scale attached to the pendulum. Its resolution is 50 nm. Since the conversion factor for the deflection is 81.9 $\frac{\mu m}{V}$, the resolution of the pendulum can be calculated to

$$\frac{50\,nm}{81.9\,\frac{\mu m}{V}} = 0.61\,mV. \tag{4}$$

The amplitude of a typical signal for an impulse measurement has a value of about 0.6 V hence the resolution of the pendulum is about 0.1 %.

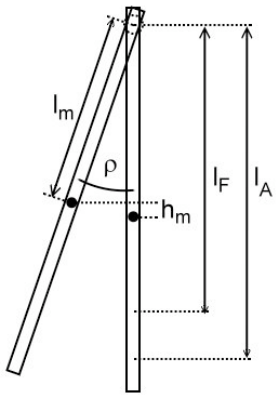

Figure 6. Schematic of Pendulum.

In order to describe the motion of a pendulum triggered by an impulse bit delivered either by the thruster or by a calibration unit the equation of energy conservation was used. Fig. 6 shows a schematic of the setup of the pendulum. During the sinusoidal motion, the energy E_I delivered by an impulse from any exciter is transformed into kinetic energy E_{kin}, potential energy E_{pot} and vibrational energy E_{vib}. The point of maximum deflection is described by the amplitude A. Here, E_{kin} is zero and E_{pot} reaches its maximum. The vibrational energy was not modeled and is neglected. Hence,

$$E_I = E_{pot} = m\,g\,h_m + \frac{1}{2}\,D\,\varphi_0^2 \tag{5}$$

describes the energy balance at that point. The center of gravity of the pendulum where the total mass m can be assumed has a distance l_m from the axis and has gained h_m in height. The energy within the torsion springs suspending the pendulum arm is stored with respect to the spring constant D and the angle of movement φ_0. Since a physical pendulum was considered, the force from the exciter onto the pendulum at the position l_F from the axis was translated into a torque acting on to the pendulum mass with moment of inertia Θ. Although the force – and hence the torque – are of course varying with time, for the calculation of the energy delivered by the exciter a constant mean force $\bar{F}$ and torque $\bar{M} = \bar{F}\, l_F$ was assumed for the duration T of the impulse. The energy from the impulse is hence

$$E_I = \frac{1}{2}\,\frac{\bar{M}^2}{\Theta}\,T^2. \tag{6}$$

Substituting equation 6 in equation 5 and solving for $I_{bit} = \bar{F}\,T$ yields

$$I_{bit} = \frac{l_m\,A}{l_F\,l_A}\,\sqrt{m\,(m\,g\,l_m + D)}. \tag{7}$$

The distance l_A was introduced to describe the point from the axis where the optical measurement takes place. In addition, the moment of inertia Θ was substituted by $\Theta = m\,l_m^2$. Eq. 6 was deduced for small angles of ϕ. It shows a linear dependency of I_{bit} and A. The center of mass l_m was calculated from the free swinging motion of the pendulum. Since all other values in the equation are known, an ideal I_{bit} can be plotted over A, for a case where no energy dissipation is assumed. For a fixed amplitude the impulse bit calculated is hence smaller than in reality.

In order to calibrate the pendulum an impulse hammer acts as exciter of the pendulum. For the impulse hammer, the distance from the axis l_F is known as well as the force acting onto the pendulum as a function of time. Thus, for the impulse hammer, the impulse bit I_{bit} can be correlated with the amplitude A measured.
However, although still promising, this method proved to be technically more involved than predicted, since the impulse hammer used in the setup did not swing onto the pendulum freely but was being pushed by a stroke magnet. This exposure to an almost constant force caused the piezo sensor to measure a force smaller than the one acting - due to the drift of the piezo crystal. The calibration of the thrust pendulum is therefore still ongoing. Values showed herein are minimal impulse, exhaust velocity and efficiency.

The measurements were recorded under $10^{-4}\ mbar$. During the measurement campaign, it was noticed that the first ten shots are not reproducible and mostly deliver a smaller impulse bit than the following ones. Hence measurements were started after $10 - 15$ preceding shots.

III. Mass Bit Measurements

The mass bit per pulse was measured by weighing the propellant bars before and after about 400 pulses performed under one parameter setting. The precision of the scale used is $10\,\mu g$. The amount of propellant ablated depends not only on the bank energy available but also on the geometry of the thruster head. Especially the ratio between h and d plays an important role. Further, the thruster circuit influences the amount of mass ablation per pulse, since late time ablation is significantly lower when the overall circuit is damped.[6] Fig. 7 shows all measurements performed with SIMP-LEX as well as mass ablation measurements of other parallel plate iMPDs found in literature[4,6,7] over a function of E_0, h and d:

$$m_{bit} = 21.4\,\sqrt{E_0}\,h\,d\,\ln\left(\frac{E_0\,d}{\sqrt{h}}\right)\,10^{-4}. \tag{8}$$

This function was found empirically in order to predict mass ablation values for modeling purposes. It shows a linear function between the x-coordinate as formulated in Eq. 8 and the mass bit.

IV. Results

Within this section, the results from variations described in Table 1 are shown. First, the influence of varying h, d and the bank energy E_0 are investigated, followed by comparison of flared and tongue shaped

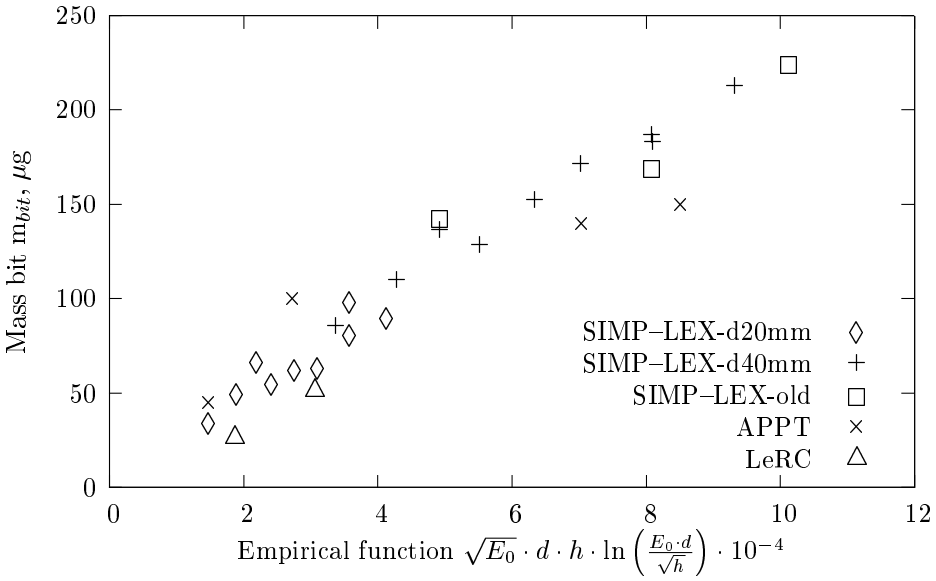

Figure 7. Mass bit over empirical energy function

electrodes with parallel, rectangular ones. Results from variation in electrode length will be presented in a later paper.

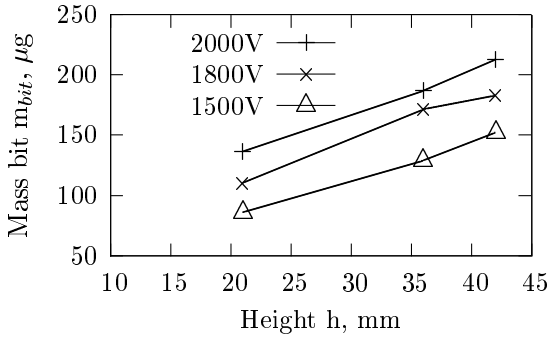

Figure 8. Mass bit over distance between electrodes for different bank energies at d=40 mm.

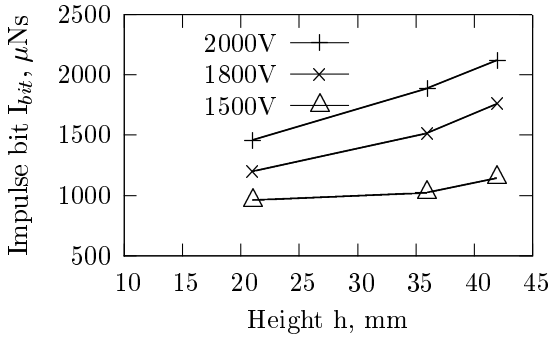

Figure 9. Minimal impulse bit over distance between electrodes for different energies at d=40 mm.

Fig. 8 shows the mean mass ablated under variation of the distance h between the electrodes for three different bank energies. These correspond to the three voltage settings investigated, $1500\,V$, $1800\,V$, $2000\,V$. The mass bit ablated increases with higher bank energies and with the distance between the electrodes. Since the graphs of all energy levels are parallel, it is assumed that

$$\frac{\partial m_{bit}}{\partial h} = \text{constant} \tag{9}$$

In addition, the mass bit also increases linearly with bank energy. This leads to the assumption, that Eq. 10 describes the general behavior of the mass bit ablated for this thruster.

$$m_{bit} = k\,E_0, \tag{10}$$

where $k = f(h)$ is a linear function of h. It must be noticed however, that this behavior changes with the circuit properties of the thruster.[6]
Fig. 9 shows the minimal impulse bit measured for the different thruster configurations with the thrust balance described above. Higher bank energies and values for h are also accompanied by an increase in the impulse bit delivered from the thruster. In Fig. 9 the slopes of the curves seem to increase with the distance

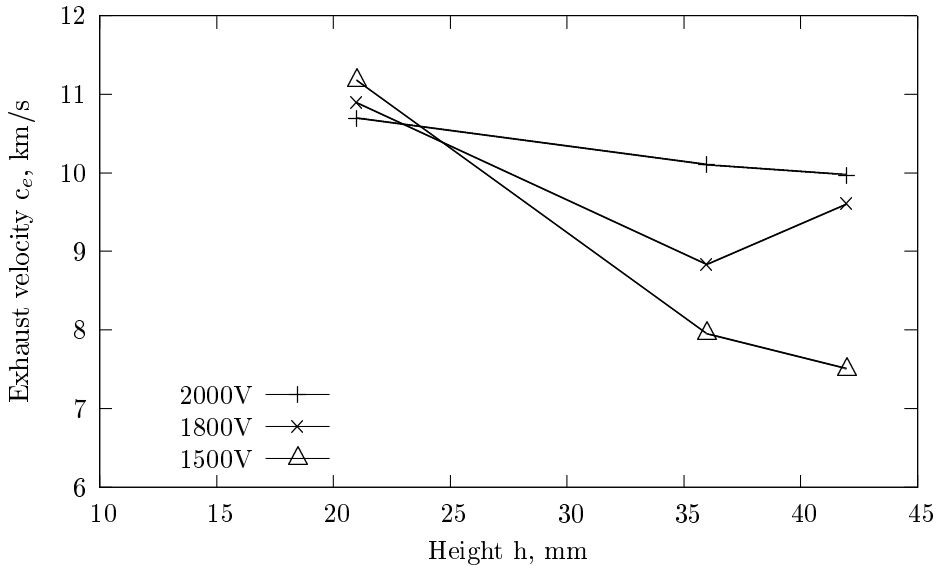

Figure 10. Minimal exhaust velocity $c_e = \frac{I_{bit}}{m_{bit}}$ over height at d=40 mm

between the electrodes. Further, the change in impulse with distance h is greater for higher bank energy levels:

$$\frac{\partial I_{bit}}{\partial h} = g(h, E_0), \tag{11}$$

where g is an increasing function of h and E_0. A change in h thus increases mass ablation while decreasing the overall acceleration of the mass bit. For lower energies, this yields only small changes in the impulse bit with varying h.
Fig. 10 shows the results obtained from mass bit and impulse bit measurements, $c_e = I_{bit}/m_{bit}$. This yields only a mean exhaust velocity over time as well as position within the exhaust plane. Hence it is not possible to derive interpretations on the velocities of each plasma sheet. All results must be regarded under this aspect. In general, a decrease in exhaust velocity is noticed with greater values of h. For higher energies however, the exhaust velocity decreases less. This is due to the steeper curve for I_{bit}: At higher energies, the increase in I_{bit} and m_{bit} are similar, hence the exhaust velocity remains almost constant. It can be observed, that the exhaust velocity is almost the same for all energy levels at $h = 21\,mm$ and $d = 40$. At $h = 40\,mm$ and $1800\,V$ the exhaust velocity seems higher than expected from the other values. It is believed that this is due to measurement errors and this configuration will be investigated again.

The influence of the bank energy toward changes in h also becomes clear when regarding Fig. 11. The change in velocity per mass bit stands for the energy deposited in mass acceleration. This value reduces significantly over h for lower energies, where at higher energies this value remains almost constant. A possible interpretation is a lack in acceleration energy for lower bank energies, due to the higher mass ablation. For higher bank energies however, there seems to be a surplus in energy at lower distances between the electrodes. Even though more mass is ablated, the change in velocity for each particle remains roughly the same.

Plotting I_{bit} over the electrode width d in Fig. 12, a maximum at $40\,mm$ can be seen for all three energy levels. These tests were conducted at 21 mm distance between the electrodes. Further tests at $h = 36\,mm$ and $h = 42\,mm$ will be carried out in order to confirm this trend.

Regarding Fig. 13 a decrease in impulse bit with higher exhaust velocities becomes clear. The point not fitting to the overall trend at $1800\,V$ is the same mentioned above for Fig. 10. It becomes apparent that the impulse bit remains almost the same for $1500\,V$ capacitor voltage, and the exhaust velocity decreases with rising h. For $2000\,V$ capacitor voltage however, it is again observed that the exhaust velocity changes much

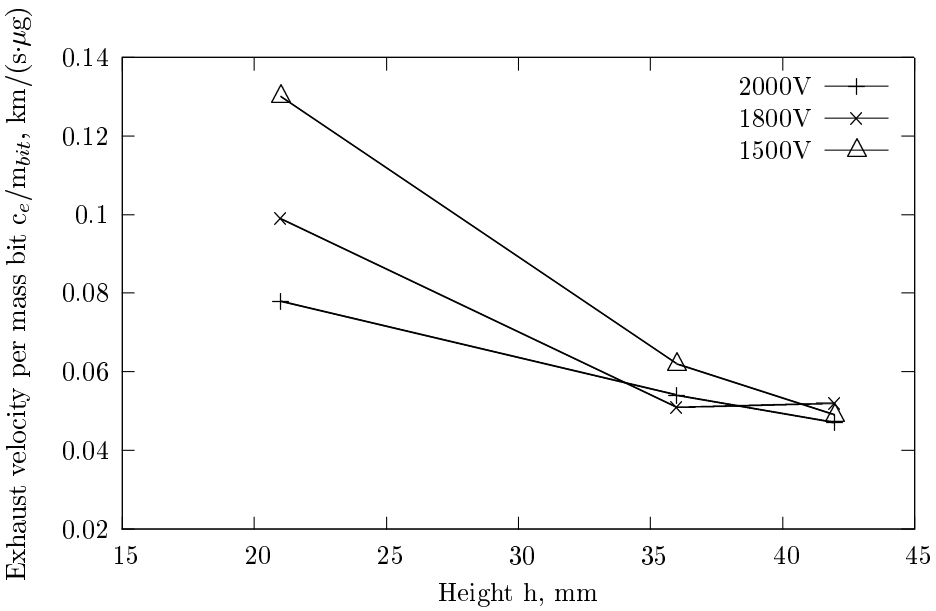

Figure 11. Minimal exhaust velocity per mass bit over height for d=40 mm

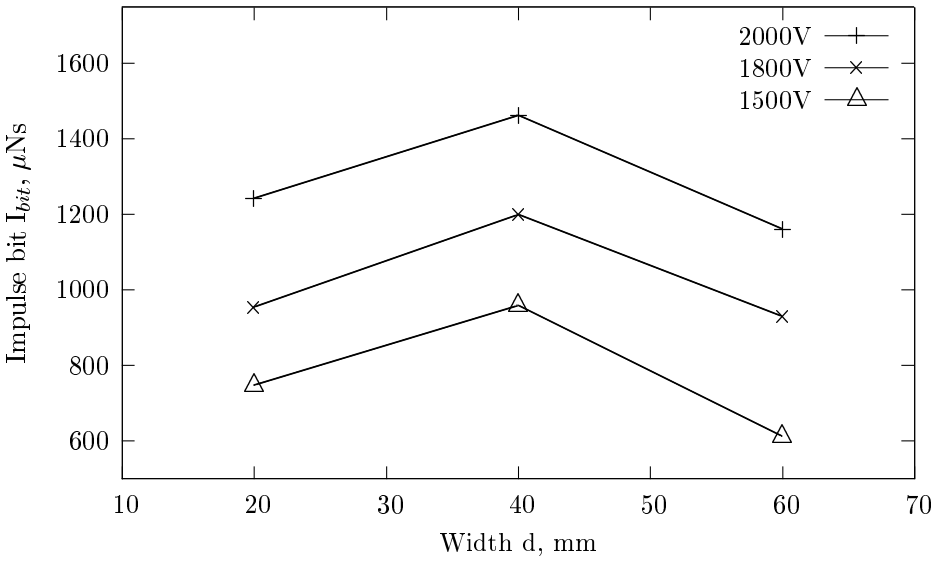

Figure 12. Minimal impulse bit over width for h=21 mm

less, but the impulse bit increases considerably with rising h. Overall, the impulse bit values are lower for lower bank energies. The maximum exhaust velocity, however, does not seem to depend on the bank energy as much as on the geometric configuration of the thruster.
Fig. 14 shows the impulse bit per projected nozzle area of the thruster over the mass bit ablated. For higher mass bits the impulse per area decreases. The graph includes all widths $d = 20\,mm$, $40\,mm$, $60\,mm$ and heights $h = 21\,mm$, $36\,mm$, $42\,mm$. The area available is not utilized efficiently anymore regarding the impulse bit for greater mass bits. Plotting $c_e^2/(2\,E_0)$ in Fig. 15 can be interpreted as the thrust efficiency per mass bit. This value is the highest for $h = 21\,mm$ at all energy levels. It is almost constant for $2000\,V$ bank energy but reduces significantly with h for $U_0 = 1500\,V$ and $U_0 = 1800\,V$. In general, the thrust efficiency per mass bit is higher for lower bank energies and lower values of h. This observation is important for optimizing the thruster toward a certain mission.

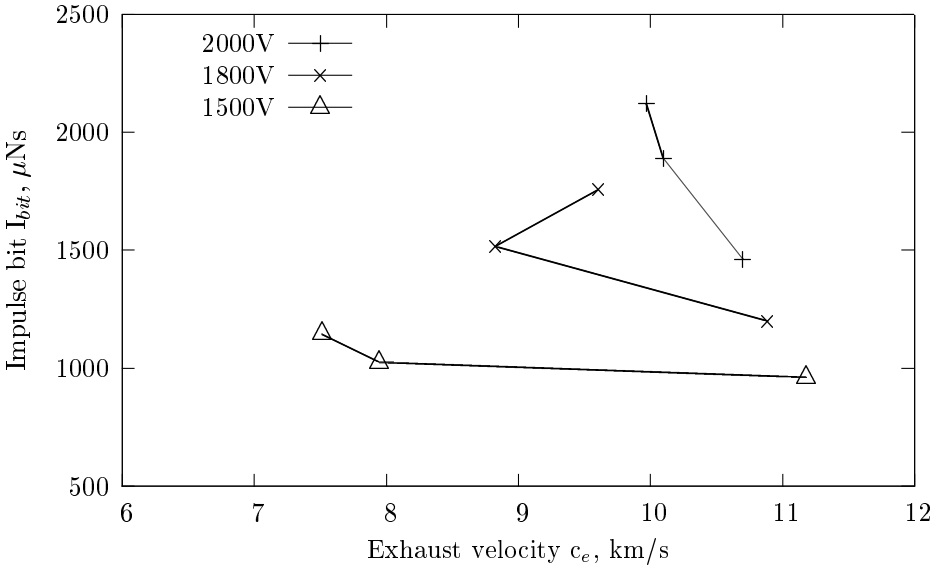

Figure 13. Minimal impulse bit over exhaust velocity for d=40 mm

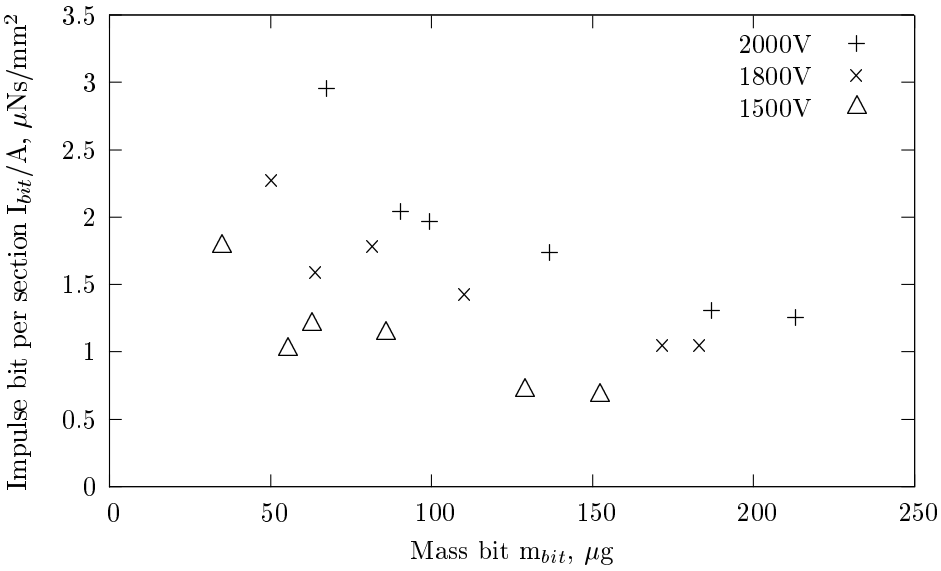

Figure 14. Minimal impulse bit per projected area $A = h\,d$ over mass bit

In order to investigate the influence of flared and tongue shaped electrodes, a width of $d = 40mm$ and

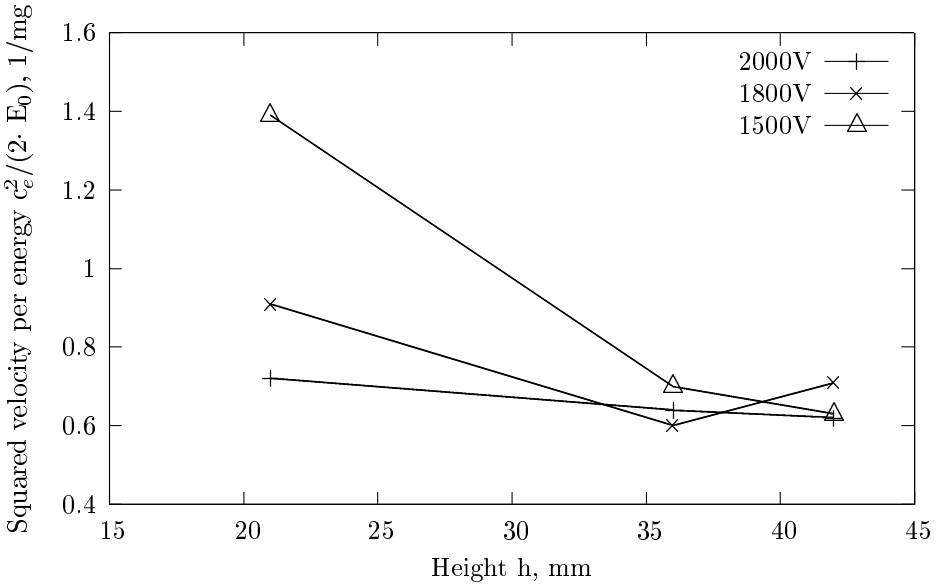

Figure 15. Minimal exhaust velocity squared per bank energy over height, translates to minimal thrust efficiency per mass bit, d=40 mm

heights of $h = 21mm$, $36mm$ were chosen. As seen in Fig. 16 the impulse bit increases by a total of about 10% with tongue and flare, compared to parallel and rectangular. The $1500\,V$ case is not comparable, since the distance between the electrodes varied. Comparing the mass bit to the values for rectangular, non-flared electrodes, no difference was found. The resulting minimal exhaust velocity shown in Fig. 17 shows a plateau for angles greater 10°. This compares well to the observations made.[8,9] Flaring the electrodes increases the exhaust velocity up to 10°. This effect is stronger for rectangular electrodes compared to tongue shaped ones. Overall however, tongue shaped electrodes yield higher exhaust velocities.

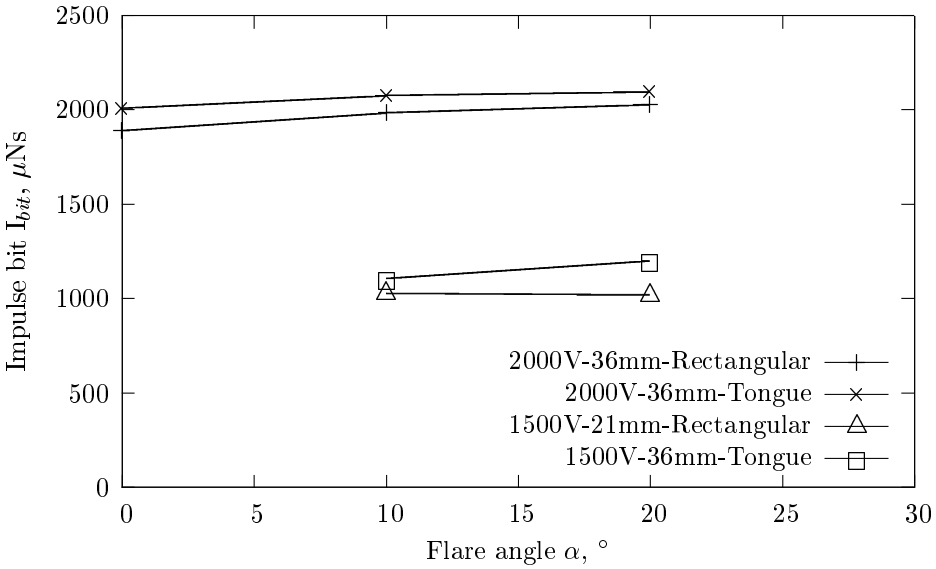

Figure 16. Minimal impulse bit over flare angle for different configurations

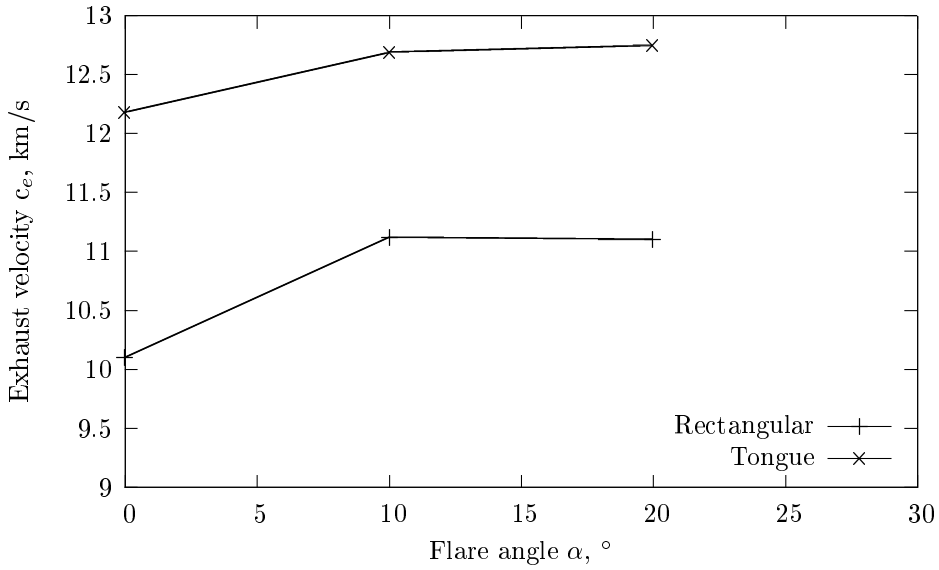

Figure 17. Minimal exhaust velocity over flare angle for d=40 mm, h=36 mm and E_0=80 J

V. Conclusion

In order to study the behavior of SIMP-LEX and characterize the influence of geometric and electric parameters, thrust balance and mass bit measurements were conducted. First, the thrust balance was studied regarding its deflection behavior. Since currently no experimental correlation between impulse bit and deflection exists, the impulse bit was deduced from the deflection measured theoretically, leading to minimal values of I_{bit} and c_e. The mean mass bit was measured over 400 pulses for all test configurations. It was found, that the mass bit can be approximated for bank energies up to $100J$ by a function of h,d and E_0. From the thrust balance measurements, an increase in impulse with h as well as with E_0 was confirmed. However, changes in h had less impact for lower bank energy levels. Further, the mean exhaust velocity $c_e = \frac{I_{bit}}{m_{bit}}$ decreases more significantly over h for lower energy levels. At higher energy levels, an increase in impulse bit can be reached without suffering significant losses in exhaust velocity. An optimum was found for the impulse bit varying the width of the electrodes at $d = 40mm$.
Using flared, tongue shaped electrodes was also investigated. Here, a maximum increase in impulse bit of 10% was found for flared and tongue shaped electrodes compared to parallel, rectangular ones. The impulse bit increases over flare angle of the electrodes. However, it was found that for more than 10° this increase levels off, and the effects might even be reversed.

Acknowledgments

This work is funded by *Deutsches Zentrum für Luft und Raumfahrt* (DLR) under contract number FKZ-50-JR-0446. The generous support regarding $Teflon$® from the PTFE specialist ElringKlinger is kindly acknowledged. The authors further want thank Mr. Bastian Steiner for conducting thrust balance tests patiently and meticulously.

References

[1]Bock, D., Auweter-Kurtz, M., Kurtz, H., Röser, H.-P., "Experimental Investigation on Thermal Arcjet Thruster Development for a Science Mission to the Moon," *57th International Congress 2006,IAC-06-C4.4.03*, Valencia, Spain, July 2007.

[2]Laufer, R., Roeser, H.-P., the Lunar Mission BW1 Project Team, "The Stuttgart Moon Orbiter Lunar Mission BW1," *Deutsche Gesellschaft für Luft und Raumfahrttechnik, Congress*, Valencia, Spain, 2007.

[3]Jahn, R.G., *Physics of Electric Propulsion*, McGraw-Hill Series in Missile And Space Technology, New York, 1968.

[4]Nawaz, A., Bauder, U., Böhrk, H., Herdrich, G., Auweter-Kurtz, M., "Electrostatic Probe and Camera Measure-

ments for Modeling the iMPD SIMP-LEX," *Joint Propulsion Conference AIAA-2007-75328*, Cincinnati, OH, July 2007.

[5]Schlipf, M., Schuster, M., *Konstruieren mit PTFE*, Verlag Moderne Industrie,Bibliothek der Technik, M¨unchen, 2nd ed., 2007.

[6]Popov, G.A., Antropov, N.N., "Ablative PPT. New Quality, New Perspectives," *Acta Astronautica*, Vol. 59, 2006.

[7]McGuire, M.L.,Myers, R.M., "Pulsed Plasma Thrusters for Small Spacecraft Attitude Control," Internal report in publication, Lewis Research Center,Cleveland, Ohio, Final Contractor Report.

[8]Palumbo, D.J., Guman, W.J., "Effects on Propellant and Electrode Geometry on Pulsed Ablative Plasma Thruster Performance," *Journal of Spacecraft and Rocket*.

[9]Palumbo, D.J.,Begun, M., "Plasma Acceleration in Pulsed Ablative Arc Discharges," Final report, Fairchild Industries Inc.